





Influences of brood-dependent behavioral variation on blue crab (*Callinectes sapidus*) larval transport in a wind-driven estuarine plume

Joseph C. Caracappa ^a  , Daphne M. Munroe ^a, Heidi L. Fuchs ^b, Robert J. Chant ^b

Show more 

 Outline |  Share  Cite

<https://doi.org/10.1016/j.ecolmodel.2023.110295> 

[Get rights and content](#) 

Under a Creative Commons [license](#) 

open access

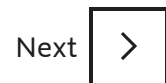
Highlights

- Blue crab larval transport was simulated within an idealized three-dimensional estuarine plume under upwelling conditions.
- Larvae had brood-dependent and individualized swimming behavior based on observations and a hypothetical behavior model.
- After 4 days of simulated transport, brood-dependent behaviors resulted in up to a 1.8 fold difference in net transport.
- Simulated larvae with behavior were transported 1.1 – 5 times further and maintained a depth 1% – 67% of passive particles in similar physical conditions.

- Despite surface-keeping behavior, the interaction between stratified currents, vertical mixing, and variation in swimming ability may be an important factor in net larval transport.

Abstract

Blue crabs (*Callinectes sapidus*) support valuable fisheries in the US mid-Atlantic Bight (MAB), and their unpredictable and variable recruitment suggests that a better understanding of larval development and dispersal is needed. Blue crab larval dispersal involves export to the continental shelf followed by re-entry of estuaries. Transport is facilitated by wind and buoyancy-driven surface currents, and zoeae generally maintain a near-surface distribution. Though several studies have investigated *C. sapidus* larval dispersal, none have evaluated the effects of behavioral variability on transport. This study simulates first-stage larvae using documented behavioral variation within an idealized wind-driven estuarine plume in order to investigate the roles of swimming behavior, stratified current systems, and turbulent mixing on transport. Model results showed that larval transport was predominately influenced by wind speed, but transport was significantly affected by behavioral characteristics. Faster swimming larvae were more able to maintain a near-surface position and had more control over their vertical position despite vertical diffusivity, and in all model scenarios, larvae travelled farther and had different vertical distributions than passive particles. Modeled net transport distance of simulated broods differed by a factor of 1.8, with a maximum 4.7 fold difference between any individual larvae, and in all scenarios behaving larvae showed further net transport and a shallower vertical distribution than passive particles. These results indicate that blue crab larval swimming ability and variability in behavioral traits may be an important factor in *C. sapidus* larval dispersal.



Keywords

Blue crab; *Callinectes sapidus*; Larval transport; Behavior; Estuary; Individual-based model

Abbreviations

MAB, Mid-Atlantic Bight; MAD, median absolute deviation; K-S, Kolmogorov-Smirnov; ANOVA, analysis of variance

1. Introduction

High inter-annual variability in blue crab (*Callinectes sapidus*) recruitment creates challenges for long-term management, and predicting patterns of larval settlement is not yet possible due to critical gaps in understanding early life stage processes. While models of *C. sapidus* larval dispersal exist for the mid-Atlantic Bight (MAB; a thorough review can be found in [Epifanio and Cohen, 2016](#)), critical knowledge gaps in early life stage processes and biophysical interactions limit our understanding of *C. sapidus* dispersal, population connectivity, and the spatial distribution of recruits. Across a variety of taxa, larval dispersal distance is inadequately explained solely by passive transport ([Kingsford et al., 2002](#); [Metaxas and Saunders, 2009](#); [Pineda and Reynolds, 2018](#)), particularly for species with long pelagic larval durations ([Shanks, 2009](#)), and larval behavior in general can greatly influence how larvae disperse ([McEdward, 1995](#); [Pineda et al., 2007](#)). Several laboratory studies have identified complex swimming behavior in *C. sapidus* larvae often regulated by environmental conditions ([Epifanio and Cohen, 2016](#); [Forward and Buswell, 1989](#); [Sulkin et al., 1980](#)), yet *C. sapidus* larval dispersal models typically treat larvae as either passive particles moving within the upper few meters of the water column ([Garvine et al., 1997](#); [Johnson and Hess, 1990](#); [Tilburg et al., 2009a](#)), or with a fixed vertical distribution of larvae ([Criales et al., 2019](#)). As yet, *C. sapidus* larval dispersal models have not considered the impact of more complex behaviors on dispersal processes.

After hatching near the mouths of estuaries, blue crab larvae (zoeae) swim to the surface and are exported onto the continental shelf, where they undergo 7 – 8 molt stages (over a 30–40 day duration) before metamorphosis ([Costlow and Bookhout, 1959](#)). Current understanding of blue crab larval dispersal in the MAB ([Epifanio and Tilburg, 2008](#)) dictates that larvae are carried southward via a near-shore buoyancy-driven surface current. Recruitment back to their parental estuary can occur when upwelling currents maintain larvae in an offshore, reducing along-shore transport ([Epifanio and Garvine, 2001](#)). Eventually, wind-driven downwelling events bring larvae back into estuarine habitats ([Epifanio and Garvine, 2001](#)). This hypothetical recruitment pathway for larvae necessitates that they remain in these surface currents to successfully reenter estuarine habitat.

Though it is often reported that blue crab zoeae exist entirely within the neuston ([Epifanio, 1995](#)), field sampling shows their vertical position can extend several meters below

the surface ([Provenzano, 1983](#); [Smyth, 1980](#)), likely due to a combination of swimming behavior and vertical mixing. Laboratory studies have demonstrated swimming responses of *C. sapidus* zoeae to temperature, salinity, light, gravity, pressure ([Forward and Buswell, 1989](#); [Sulkin et al., 1980](#)), as well as turbulence in megalopae ([Welch et al., 1999](#)). Early-stage larvae exhibit negative geotaxis and high barokinesis, resulting in continual upward swimming ([Sulkin 1984](#)). *In situ*, zoeae presumably stop swimming for some time and resume swimming once triggered by depth or time-dependent cues. Additionally, since zoeae occupy the turbulent surface mixed layer, vertical mixing should prevent zoeae from staying exclusively within the neuston.

C. sapidus zoeal swimming ability is a function of both behavior and morphology. Zoeal swimming appendage length is an indicator of vertical velocity, the verticality and straightness of swimming trajectories, while dorsal cross-sectional area is a strong indicator of maximum swimming speed ([Caracappa and Munroe, 2019](#)). Recent work has shown that the offspring of different female crabs (broods) can differ in both morphological and behavioral characteristics ([Caracappa and Munroe, 2019, 2018](#)). Zoeae from different broods have been observed to swim at speeds varying by a factor of three, which was partially explained by corresponding differences in morphology. ([Caracappa and Munroe, 2019](#)) Despite natural variation in traits being expected within a population, when combined with the physical processes of dispersal, the resulting larval transport patterns may partially depend on a zoea's parentage. The potential for maternal influences to affect offsprings' dispersal trajectories may have further implications on blue crab metapopulation dynamics. Specifically, female crabs in the same location could contribute to settling habitats differently by virtue of their offsprings' behavioral and morphological characteristics.

C. sapidus larvae develop on the inner continental shelf in the MAB, where circulation is primarily governed by the buoyant outflow of large riverine estuaries and wind-driven Ekman dynamics ([Garvine et al., 1997](#)) with an overlaying southwest mean current ([Lentz, 2008](#); [Yankovsky et al., 2000](#)). The southward elongation of these estuarine plumes creates a fresher and stratified region where zoeae are often retained ([Ruzecki, 1981](#)). Episodic and seasonal changes in wind direction can cause offshore or inshore transport of near-surface waters and result in retention or expulsion of zoeae from the proximity of natal estuaries ([Epifanio, 1995](#)). Additionally, vertically sheared currents can be generated by wind-stress and friction ([Craig, 1996](#); [Richman et al., 1987](#)), and wind stress and breaking waves result in an increasing vertical diffusivity with depth, influencing the larval vertical position ([Visser, 1997](#)).

Several studies have modeled *Callinectes sapidus* larval dispersal in the MAB, but to our knowledge none have considered the effects of complex individualized behaviors. Early models of *C. sapidus* dispersal involved Lagrangian transport of buoyant particles near the mouth of Cheapeake Bay ([Johnson, 1985](#); [Johnson et al., 1984](#)), identifying the importance of wind-driven and buoyancy-driven features in particle transport. Improvements to similar models sought to provide possible reinvasion mechanisms for blue crab larvae ([Garvine et al., 1997](#); [Johnson and Hess, 1990](#)). Later studies, using improved circulation models, proposed possible offshore retention of zoeae such that groups of larvae can stay relatively close to natal estuaries and facilitate later reinvasion ([Tilburget al., 2009b, 2007, 2005](#)). More recent models have shown success with incorporating behaving ([Crialet al., 2019](#)) and surface-drifting ([Giltz et al., 2020](#)) particles, though larval behavior was treated as uniform.

The goal of this study was to use model simulations of an idealized estuarine plume over the continental shelf in order to explore how behavioral-physical interactions may influence the transport of *C. sapidus* larvae, while incorporating recent observational and experimental data. Our objectives were to (1) formulate a hypothetical larval behavior model for first-stage *C. sapidus* zoeae, (2) estimate the degree to which larval behaviors influence transport with respect to passive transport, and (3) quantify the effects of brood-level behavioral differences on larval transport.

2. Materials and methods

2.1. Model design

All parameter names and definitions are listed in [Table 1](#). The following idealized physical simulation was chosen over more complex modeling frameworks like ROMS as the behaviors investigated in this study require a near-surface vertical resolution on a centimeter scale, much smaller than existing ROMS products for the region. The development of a higher resolution product would have been impractical without adequate support that such behaviors are relevant for *C. sapidus* larval dispersal processes. Larval transport was simulated in an idealized two-layer estuarine plume in upwelling conditions over a continental shelf with an unbounded horizontal plane and a depth of 50m. Horizontal advection was driven entirely by a wind-driven Ekman velocity profile under constant northward wind-stress. Simulations were set to be in the northern hemisphere with positive x (U velocity) as eastward (along-plume), and positive y (V velocity) as northward (across-plume). Other vertical processes (e.g. upwelling and downwelling) events have been shown to influence larval settlement ([Epifanio and Garvine, 2001](#);

Shanks and Brink, 2005; Sponaugle et al., 2002), they occur at speeds that would dominate over any larval behaviors. As such, no vertical advection was present besides for that generated from vertical diffusivity to more easily isolate behavior effects in conditions where larvae are more likely to have control over their vertical position.

Table 1. Model parameter definitions and values, if constant.

Variable	Name	Units/Value	Equation
A_A	Larval anterior cross-sectional area	m^2	
A_D	Larval dorsal cross-sectional area	m^2	
C_D	Drag coefficient		7
D_{max}	Larval swimming depth trigger	m	
f	Coriolis parameter	$10^{-4} s^{-1}$	
g	Gravitational acceleration	$9.8 m s^{-2}$	
H	Water column depth	50m	
κ	Von Kármán constant	0.4	
K_z	Vertical diffusivity	$m^2 s^{-1}$	4
L_c	Larval carapace length	m	
ρ	Below-plume seawater density	$1023 kg m^{-3}$	
ρ_0	Surface seawater density	$1019 kg m^{-3}$	
ρ_L	Larval density	$1066 kg m^{-3}$	
Pe	Péclet number		11
r	Variance of R	1/3	
R	Uniform random variable between -1 and 1		
Re	Reynolds number		8
Ri	Bulk Richardson Number	1	
S	Net transport distance	m	
S_{max}	Maximum theoretical transport	m	12
τ	Wind stress	$N m^{-3}$	

Variable	Name	Units/Value	Equation
Δt	Model time step	1 s	
U	Eastward velocity	m s^{-1}	2
u^*	Shear velocity	m s^{-1}	5
μ	Dynamic viscosity of seawater	$0.001 \text{ kg m}^{-1} \text{ s}^{-1}$	
V	Northward velocity	m s^{-1}	3
V_L	Larval volume	m^3	
W_p	Particle velocity (swimming or sinking)	m s^{-1}	
W_{swim}	Upward larval swimming velocity	m s^{-1}	
W_{sink}	Larval passive sinking velocity	m s^{-1}	6
X_{net}	Net x-transport	M	
Y_{net}	Net y-transport	M	
z	Depth	M	
z_p	Plume Depth	m	1

The depth of the estuarine plume (z_p) was defined using a model by [Fong and Geyer \(2001\)](#), which was developed to investigate the dynamics of riverine plumes similar to that occupied by *C. sapidus* zoeae in the MAB.

$$z_p = \left[\frac{4Ri_c \left(\frac{\tau}{f\rho_0} \right)^2}{g \left(\frac{\rho - \rho_0}{\rho} \right)} \right]^{\frac{1}{3}} \quad (1)$$

where ρ_0 is the mean density of seawater within the plume (1019 kg m^{-3}), ρ is the density of the bottom layer (1023 kg m^{-3}), g is the gravitation acceleration (9.8 m s^{-2}), f is the Coriolis parameter (10^{-4} s^{-1}), Ri_c is a critical bulk Richardson Number in the range of 0.5–1.1 but assumed to be 1 ([Pollard et al., 1973](#); [Price et al., 1978](#)), and τ is the wind stress. τ was estimated from free-stream wind speed using an empirical relationship ([Large and Pond, 1980](#)). Plume and below-plume densities were estimated from observations ([Whitney and Garvine, 2005](#)), and while measured before typical spawning (April–May), they provide a reasonable upper bound on annual plume stratification (although not necessarily representative of extreme events or climatological averages). Given the high interannual

variability in estuarine export (Jiang and Xia, 2016), it may be necessary to simulate a dynamic plume depth in future iterations.

Horizontal velocity profiles were then defined as a steady-state Ekman system with a constant northward wind (Pond and Pickard, 1983)

$$U(z) = \frac{\sqrt{2\pi\tau}}{z_p \rho_0 |f|} \cos\left(\frac{\pi}{4} + \frac{\pi}{z_p} z\right) e^{\frac{\pi}{z_p} z} \quad (2)$$

$$V(z) = \frac{\sqrt{2\pi\tau}}{z_p \rho_0 |f|} \sin\left(\frac{\pi}{4} + \frac{\pi}{z_p} z\right) e^{\frac{\pi}{z_p} z} \quad (3)$$

where z is the depth in meters. The usage of z_p as the Ekman depth constrains the flow to within the estuarine plume.

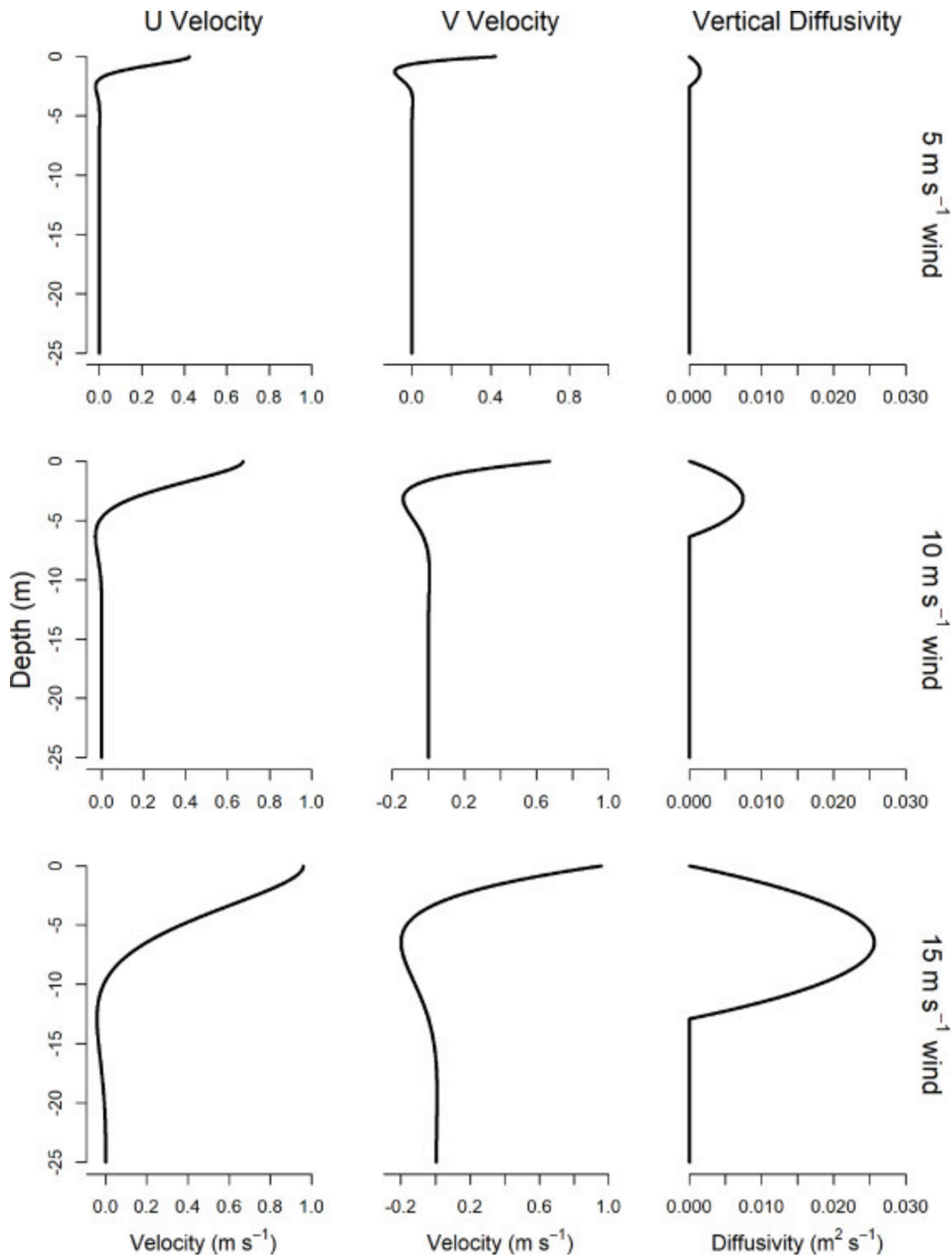
A vertical diffusivity (K_z) profile was also specified by

$$K_z = \begin{cases} u_* \kappa z \left(\frac{H-z}{H}\right) & -z_p \leq z \leq 0 \\ 5 \times 10^{-6} & z < -z_p \end{cases} \quad (4)$$

where κ is the Von Kármán constant (0.4), H is the water column depth (50m), and u_* is the shear velocity defined by

$$u_* = \sqrt{\frac{\tau}{\rho_0}} \quad (5)$$

A background diffusivity of $5 \times 10^{-6} \text{ m}^2 \text{ s}^{-1}$ was based on a model by Fong and Geyer (2001). This parameterization of K_z produced a differentiable diffusivity profile as a function of wind speed with a maximum K_z at $\frac{z_p}{2}$ and a maximum $\frac{dK_z}{dz}$ at the surface and z_p . A cubic spline was used to create a smooth but rapid transition in K_z at the plume interface (i.e. pycnocline). Three physical scenarios were used that had unique K_z and velocity profiles (Fig. 1) each using a different constant wind speed (5 m s^{-1} , 10 m s^{-1} , 15 m s^{-1}). These speeds encompass the range in observations by the NOAA NDBC CMAN4 station in the mouth of Delaware Bay, USA (<https://www.ndbc.noaa.gov>). It was within each of these physical scenarios that various larval behavior configurations were investigated.



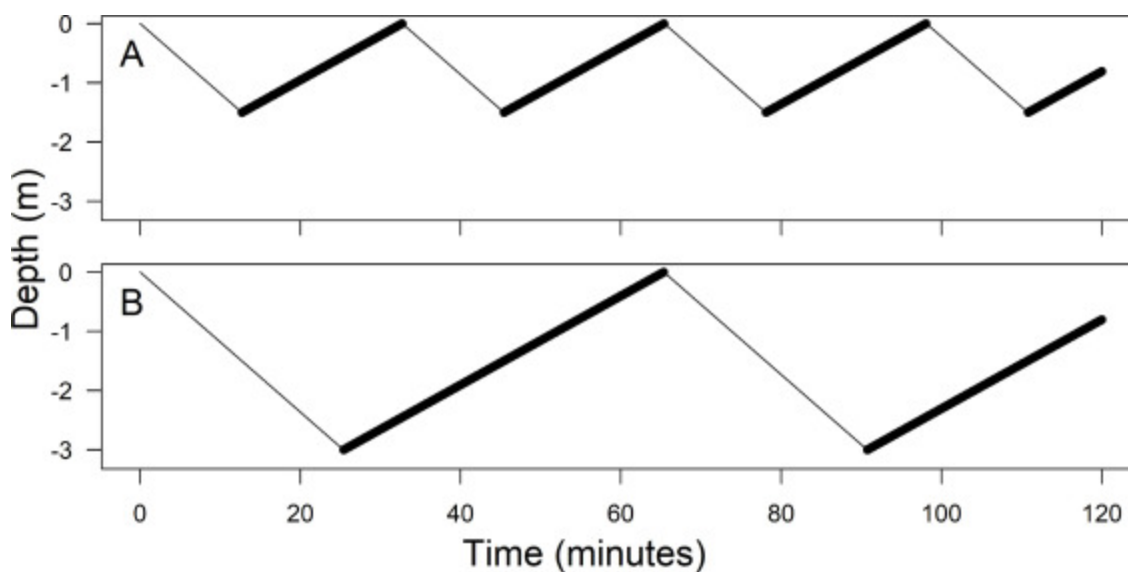
[Download: Download high-res image \(553KB\)](#)

[Download: Download full-size image](#)

Fig. 1. Simulated vertical profiles of U velocity (left column), V velocity (center column), and vertical diffusivity (right column) for each of the 3 wind speed scenarios (rows).

2.2. Larval behavior

The in situ swimming behavior of *C. sapidus* zoeae has not been well-documented on short time-scales, so a two-phased hypothetical behavioral model was used that includes elements of both laboratory and field observations. This behavioral model presumes that while generally surface keeping, *C. sapidus* zoeae cease swimming periodically and are cued to resume swimming by a depth cue. These short oscillations have been observed in laboratory conditions (Caracappa and Munroe, 2019), but have not been measured in the coastal ocean. In the first phase, larvae sink passively until they reach a hypothetical depth trigger (D_{max}). The hypothetical D_{max} parameter aims to reproduce a barokinetic response documented in laboratory settings (Sulkin et al., 1980) but as a discrete environmental cue. Once reaching a depth of D_{max} , a second swimming phase begins where larvae swim upwards until reaching the surface. Since the value D_{max} is uncertain, three possible values (0, 1.5, and 3 m) were used, encompassing the vertical distribution of observed zoeae (Provenzano, 1983). In a still water column, larvae with a nonzero D_{max} will vertically oscillate between the surface and their D_{max} in a sawtooth pattern (Fig. 2). Thus given a fixed swimming and sinking velocity, D_{max} also determines the frequency of particles' vertical oscillations. This behavior differs from depth tracking, as there is no evidence that larvae aggregate at any non-surface depths, but it does represent a type of depth-regulation, whereby larvae swim such that they stay above, rather than at, their D_{max} . A D_{max} of 0 m results in constant upward swimming regardless of depth with no passive sinking phase. As a hypothetical parameter, $D_{max}=0$ m is treated as a control. In the absence of turbulence, particles would behave as buoyant surface drifters.

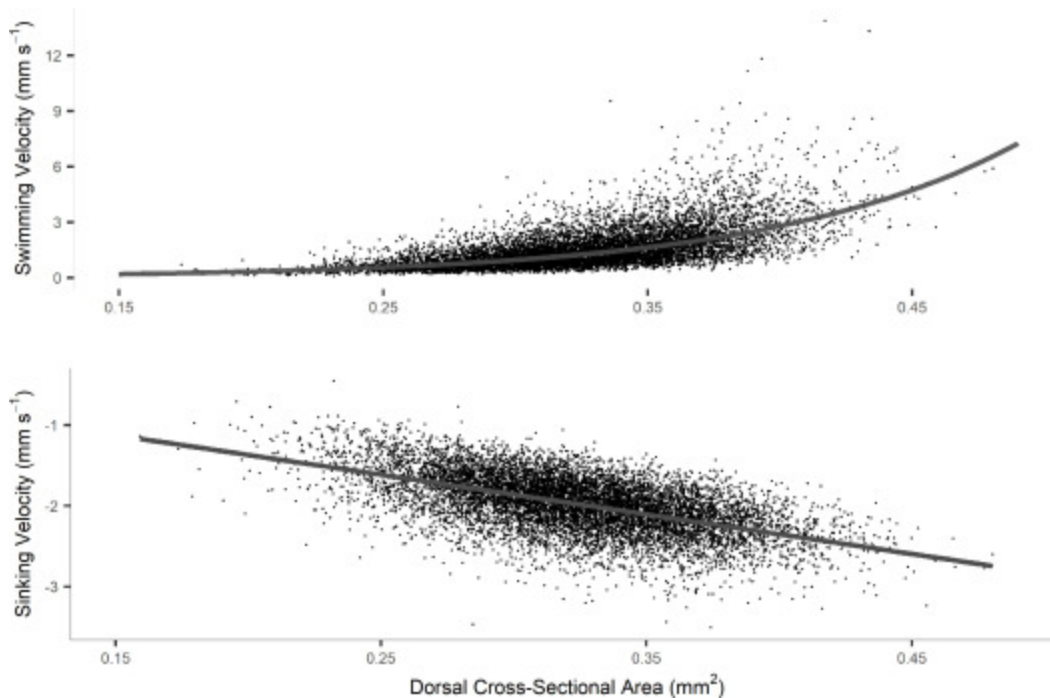


[Download: Download high-res image \(198KB\)](#)

[Download: Download full-size image](#)

Fig. 2. Hypothetical larval swimming behavior in absence of turbulence shown as depth over time for larvae with the same swimming and sinking velocities but a D_{\max} of 1.5 m (A) and 3 m (B). Thicker segments show phases when larvae are swimming upward.

Observations show that first-stage *C. sapidus* zoeae exhibit significant brood-dependent morphology and swimming behavior (Caracappa and Munroe, 2019, 2018). Empirical relationships between swimming velocity and morphology were used to generate distributions of possible behaviors, as there is no available data on paired swimming and sinking observations for individual larvae within a single brood. Four larval broods from Caracappa & Munroe (2019) (denoted groups A through D) were used to generate behaviors. These broods were selected due to their significant differences in both swimming velocity and morphology. A composite group using the combined distribution of all larvae measured in Caracappa and Munroe (2019) was also used (group O), totaling 5 larval groups. Individual swimming and sinking velocities were generated from the dorsal cross-sectional area (A_D), a highly correlated morphometric. Upward swimming velocity (W_{swim}) was best approximated an exponential function of A_D and a normally distributed error term with a mean of 0 and a standard deviation equal to that of the residuals of the regression (Fig. 3, Table 2). An exponential relationship was chosen to constrain W_{swim} to positive values. A random value of A_D was drawn for each larvae based on observed distributions within each group, and a corresponding W_{swim} was generated.



[Download: Download high-res image \(461KB\)](#)

[Download: Download full-size image](#)

Fig. 3. Relationship between dorsal cross-sectional area (A_D) and larval swimming (top) and sinking (bottom) velocity based on data from [Caracappa and Munroe \(2019\)](#). Solid lines show the results of the log-linear regression for swimming velocity ($R^2=0.39$, $p<0.001$) and the linear regression for sinking velocity ($R^2=0.30$, $p<<0.001$). Both show larvae from the overall distribution (group O).

Table 2. Empirical relationships between morphological and behavioral traits.

Equation	R^2	p
$W_{swim} = 0.04e^{1.06 \times 10^7 A_D + \epsilon}$	0.41	$<<0.001$
$A_A = 0.58A_D + 4.32 \times 10^{-8} + \epsilon$	0.68	$<<0.001$
$L_C = 534A_D + 2.04 \times 10^{-4} + \epsilon$	0.46	$<<0.001$
$V_T = 1.57 \times 10^{-4} - 1.08 \times 10^{-11} + \epsilon$	0.70	$<<0.001$

Sinking velocity (W_{sink}) was estimated using morphology and a force balance including drag, gravitational sinking, and buoyancy:

$$W_{sink} = \sqrt{\frac{2gV_L(\rho_L - \rho_f)}{\rho_f A_A C_D}} \quad (6)$$

where g is the gravitational acceleration (9.8 m s^{-2}), ρ_L is the density of larvae (1066 kg m^{-3} : Fuchs and Low, unpublished data.), V_L is an estimate of larval volume, and A_A is the anterior cross-sectional area of larvae (in their sinking orientation). Estimates of V_L assume an ellipsoidal carapace where $V_L = \frac{4}{3}\pi \text{ length} \times \text{width} \times \text{height}$ ([Caracappa and Munroe, 2018](#)). C_D is the drag coefficient, for which we use the formula of [White \(1974\)](#):

$$C_D = \frac{24}{Re} + \frac{6}{1 + \sqrt{Re}} + 0.4 \quad (7)$$

Re is the Reynolds number, defined as

$$Re = \frac{L_C W_{sink} \rho_o}{\mu} \quad (8)$$

where L_C is the carapace length of larvae, and μ is the dynamic viscosity of seawater ($0.001 \text{ m}^{-1}\text{s}^{-1}$). This formulation of C_D is valid for objects with Re from 1 to 2×10^5 ([White, 1974](#)) and encompasses the typical Re range for zoeae including *C. sapidus* (0.6 to 10 based on estimates from [Caracappa and Munroe, 2019](#)). Linear regressions were used to generate A_A ,

L_C , and V_T for each larvae as a function of A_D (Table 2). This allowed for individual and brood variation in W_{sink} and W_{swim} to be generated from the same morphometric data (Table 3).

Table 3. Swimming (W_{swim}) and sinking (W_{sink}) velocity of each larval group.

Larval group	W_{swim} (\pm sd) (mm s ⁻¹)	W_{sink} (\pm sd) (mm s ⁻¹)
A	1.54 (1.09)	-1.98 (0.35)
B	3.00 (1.86)	-2.29 (0.30)
C	2.05 (1.27)	-2.13 (0.31)
D	1.34 (0.80)	-1.94 (0.31)
O	1.15 (0.71)	-1.87 (0.33)

2.3. Inclusion of turbulent motion

Simulated particles moved individually and exhibited vertical motion based on a turbulence-behavior model by Ross & Sharples (2004) which accounts for spatially non-uniform diffusivity. This discrete-time equation determines the particle depth at the next timestep (z_{n+1}) based on its current depth (z_n)

$$z_{n+1} = z_n + \frac{\delta K_z(z_n)}{\delta z} \Delta t + R \left[\frac{2}{r} K_z \left(z_n + \frac{1}{2} \frac{\delta K_z(z_n)}{\delta z} \Delta t \right) \Delta t \right]^{1/2} + W_p \Delta t \quad (9)$$

where Δt is the discrete time increment (1 s), R is a uniformly distributed random number between -1 and 1 , r is the variance of R ($1/3$), and W_p is the directed particle velocity (W_{swim} or W_{sink}) depending on the behavioral phase. The second term is deterministic and moves particles towards depths of increased diffusivity (i.e. towards mid-plume depths). The third term is a stochastic and nonlinear process with a random direction and increasing magnitude with depth. The final term represents the directed motion of larvae. A simple reflective boundary was used such that if particles were transported vertically beyond the top or bottom boundary in the next timestep, they were reflected proportionally inward.

$$z_{n+1} = \begin{cases} -z_n & z_{n+1} > 0 \\ 2H + z_{n+1} & z_{n+1} < -H \end{cases} \quad (10)$$

To more clearly distinguish the interactions between physical processes and larval behaviors, the only physical processes acting on simulated larvae were vertical diffusivity and horizontal currents. For all simulations, horizontal diffusivity was absent as it would have affected all larvae equally regardless of behavior.

2.4. Model implementation and analysis

All simulations and statistical analyses were implemented in R (R [CoreTeam, 2015](#)). In each model configuration, 10,000 particles were released at the same horizontal position at 1 m depth and their x-y-z position was tracked for 4 simulated days, the typical duration of first stage *C. sapidus* zoeae ([Costlow and Bookhout, 1959](#)). Only first stage processes were considered since individualized swimming behaviors have not been reported for older zoeae. The number of particles exceeds that needed to reach less than 5% unexplained variance ([Simonsetal., 2013](#)) and allowed for a smooth distribution of particle positions. A timestep of 1 s was used, meeting criteria proposed by [Ross and Sharples \(2004\)](#), and positional data was recorded every 10 min. The net horizontal transport (S) was then calculated as the Euclidean distance between the final and initial x-y coordinates (excluding differences in vertical position). The net transport in the x (along-plume) and y (cross-plume) directions were also calculated as X_{net} and Y_{net} , respectively. Since transport metrics were not normally distributed, a median was used as the central statistic with the median absolute deviation (MAD) as a measure of dispersion. Net transport is not always the most relevant metric when predicting the larval recruitment ([Pinedaetal., 2007](#)), but it provides a useful indicator as to the degree that behavioral characteristics influence particle transport in a semi-uniform physical environment.

The Péclet number (Pe) was calculated for all particles in each model configuration. Pe is a dimensionless metric relating to the ratio of diffusive and advective forces and can be used as an indicator of the dominant forces acting on swimming plankton ([Karp-Bossetal., 1996](#)). Pe is defined as

$$Pe = \frac{z_p W_{swim}}{\overline{K_z}} \quad (11)$$

Where $\overline{K_z}$ is the depth-averaged between the surface and z_p . The fraction of simulated larvae with $Pe > 1$ was used to indicate whether larval motion during a given configuration was dominated by behavior or turbulence.

Two distinct model scenarios were constructed, each with several distinct physical and behavioral configurations. In the *behavior scenario*, particles had active swimming behaviors, with 45 configurations including all combinations of wind speed (3), D_{max} (3), and larval group (5). In the *passive scenario*, simulated larvae were neutrally buoyant and possessed no behavior ($W_{swim} = 0 \text{ms}^{-1}$ and $W_{sink} = 0 \text{ms}^{-1}$). The *passive scenario* acted as a control for swimming behavior and included configurations for each of the three wind speeds.

For each scenario, an ANOVA was used to determine whether S differed between configurations of wind speed, D_{max} , and larval group. Kolmogorov-Smirnov (K-S) tests were used to determine whether the distribution of S from configurations with behaving particles differed from the corresponding configuration with passive particles but the same physics. An ANOVA was used to determine whether the mean vertical position of particles at the final time step differed between model configurations. K-S tests were also used to evaluate whether mean particle depth differed in configurations with and without larval behavior.

The maximum theoretical transport (S_{max}) was calculated for each combination of wind speed and D_{max} by evaluating the horizontal advection at one-half D_{max}

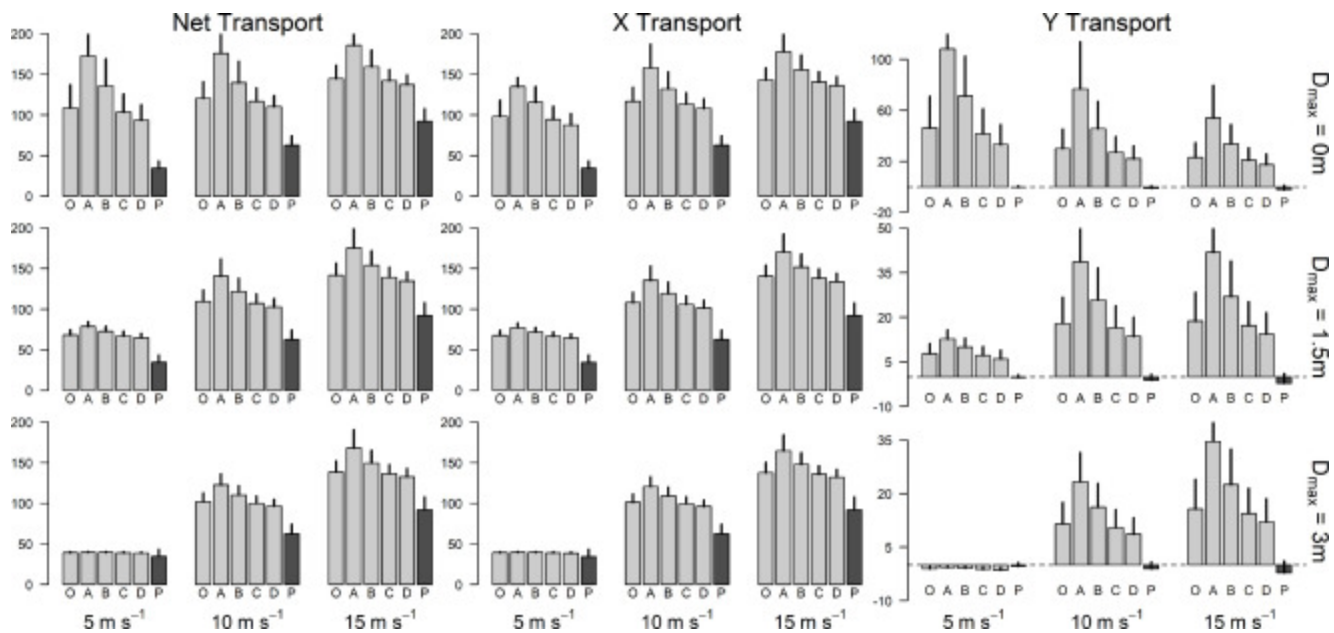
$$S_{max} = t_{tot} \sqrt{U \left(\frac{D_{max}}{2} \right)^2 + V \left(\frac{D_{max}}{2} \right)^2} \quad (12)$$

where t_{tot} is the total duration of the simulation (4 days). This metric represents the mean horizontal advection a behaving particle would experience in the absence of turbulence. Due to the parameterization of the behavioral model, any particle with D_{max} greater than 0m would have a subsurface mean depth, even if W_{swim} was high. Thus S_{max} is not equivalent to surface transport, and provides a simple reference point to compare to realized net transport (S) and quantify the effect of turbulence on behaving particles.

3. Results

3.1. Behaving particle scenarios

For model configurations with behaving particles, wind speed was the dominant factor, where increased wind speed resulted in further transport in all cases (Fig. 4). This was expected given that the mean current velocity scales with $\tau^{1/3}$. A 3-factor ANOVA ($S \sim \text{Wind} \times D_{max} \times \text{Larval Group}$; Table 4) showed a significant interaction between wind speed and D_{max} . When $D_{max}=0\text{m}$, faster swimming larvae stay nearer to the surface at low wind speeds (Fig. 5) and thus behave more like buoyant surface drifters. As D_{max} increases, net transport and its variability decline (Table 5), since larvae spend more time in deeper, slower moving horizontal currents. Larval groups had significant effects on transport distances, especially when $D_{max}=0\text{m}$. Faster swimming broods were able to stay closer to the surface and transport further regardless of higher K_z during stronger wind stress configurations. As D_{max} increased, particles were more evenly mixed vertically throughout the plume (Fig. 5), and the brood effect was diminished. When wind speed and K_z increased, brood difference in transport also increased.



[Download: Download high-res image \(470KB\)](#)

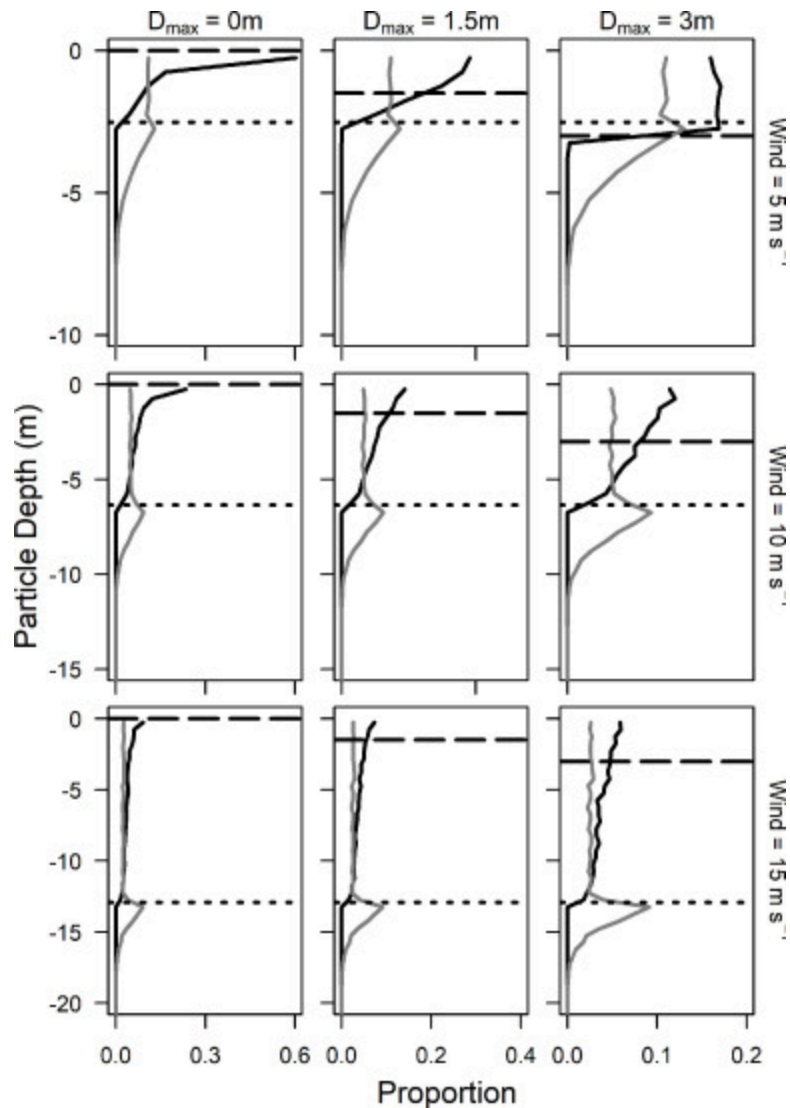
[Download: Download full-size image](#)

Fig. 4. Net (left column), X (center column), and Y (right column) particle transport distance was calculated for each D_{max} value (rows). Each panel depicts the associated transport distance for the three wind speed scenarios (5 m s^{-1} , left; 10 m s^{-1} , center; 15 m s^{-1} , right). The median transport distance for each larval group is shown by light gray bars; error bars showing the median absolute deviation ($N=10,000$). Corresponding transport distance for the same model configuration without behavior (i.e. the passive model) is shown by the dark gray bar.

Table 4. Results of 4-way ANOVA on net transport distance in the Behavior Model scenario. P values are adjusted using a Bonferroni correction (90 comparisons).

	Df	Mean square	F	p	Effect size
Wind	2	2.27×10^8	2.74×10^5	$\ll 0.001$	0.385
D_{max}	2	7.93×10^7	9.54×10^4	$\ll 0.001$	0.134
Larval Group	4	2.27×10^7	2.73×10^4	$\ll 0.001$	0.077
Wind \times D_{max}	4	1.85×10^7	2.23×10^4	$\ll 0.001$	0.063
Wind \times Larval Group	8	7.90×10^5	951	$\ll 0.001$	0.005
$D_{max} \times$ Larval Group	8	2.38×10^6	2863	$\ll 0.001$	0.016

	Df	Mean square	F	p	Effect size
Wind×D_{max}×Larval Group	16	1.86×10 ⁵	224	≪0.001	0.003
Residuals	449,955	830			



[Download: Download high-res image \(368KB\)](#)

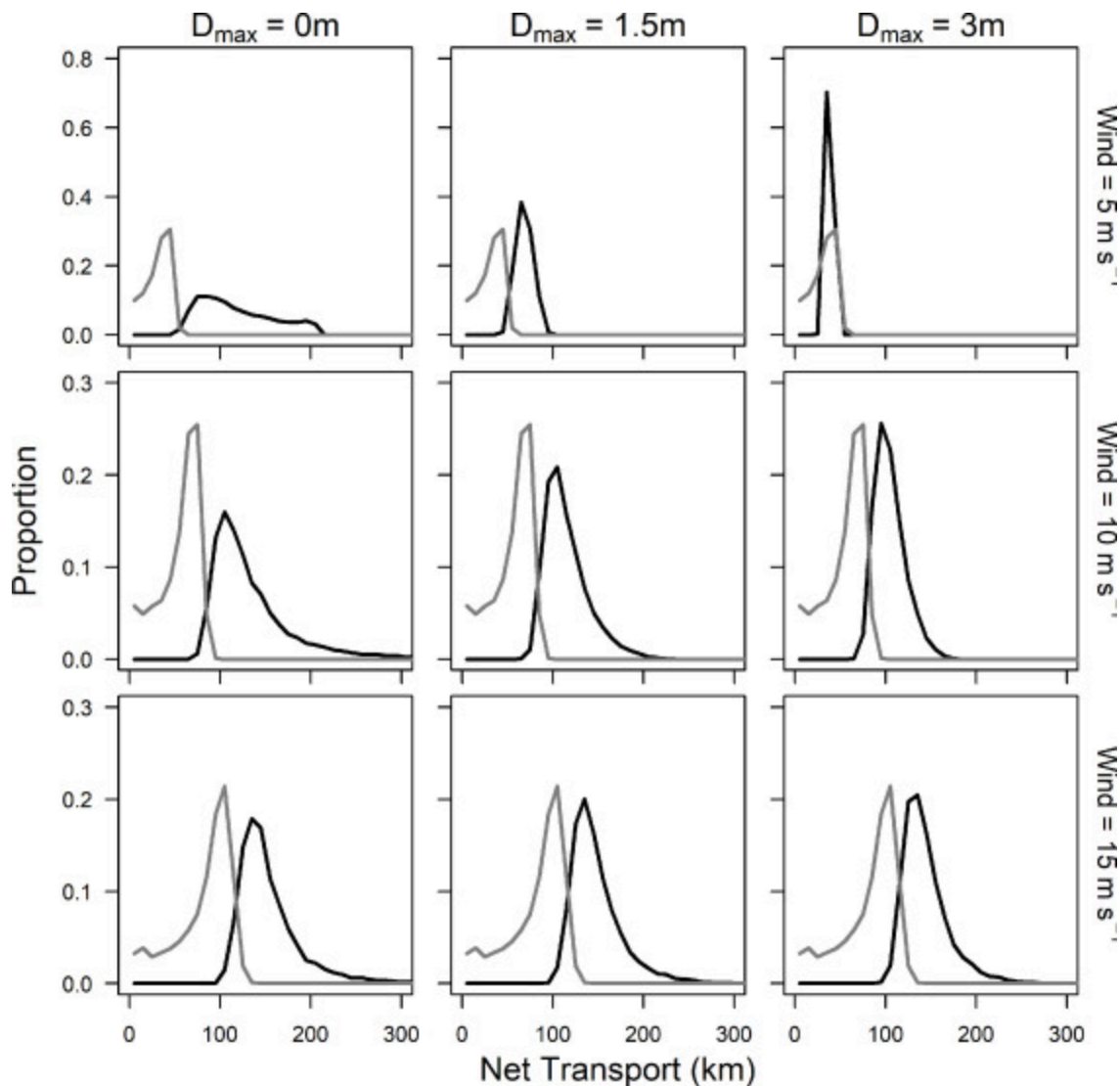
[Download: Download full-size image](#)

Fig. 5. The proportion of particles within 1 m depth bins for the “O” group with behavior (black lines) and passive particles (grey lines). Horizontal dotted lines show the plume depth at each configuration. Horizontal dashed lines show D_{max} depth. Frequencies are divided by D_{max} values (columns) and wind speeds (rows).

Table 5. Summary of mean net transport and particle depth for model configurations with behaving and passive particles. Values in parentheses show one standard deviation.

D_{max}	Wind speed (m s ⁻¹)	Net transport (km)			Final depth (m)		
		Behaving larvae	Passive larvae	Behaving/Passive	Behaving larvae	Passive larvae	Behaving/Passive
0	5	108.5 (28.5)	34.4 (9.0)	3.16	-0.3 (0.3)	-2.3 (1.1)	0.13
1.5		68.1 (6.5)		1.98	-0.9 (0.5)		0.39
3		39.2 (1.1)		1.14	-1.5 (0.7)		0.66
0	10	120.5 (20.3)	62.6 (11.6)	1.93	-1.8 (1.4)	-5.0 (2.1)	0.36
1.5		109.6 (14.0)		1.75	-2.1 (1.3)		0.42
3		102.0 (10.7)		1.63	-2.3 (1.4)		0.47
0	15	144.9 (16.4)	92.1 (15.6)	1.57	-4.7 (3.1)	-9.7 (4.0)	0.49
1.5		141.7 (14.8)		1.54	-4.8 (3.0)		0.49
3		138.6 (13.4)		1.50	-5.0 (3.0)		0.51

For each larval group, S showed a unimodal and a semi-symmetrical distribution for particles with a non-surface D_{max} (Fig.6). Particles with $D_{max}=0$ m had more skewed distributions and median transport differed between larval groups. The fasting swimming group (A) was transported significantly further than all other groups (K-S test, $p \ll 0.001$). As wind speed increased median vertical position decreased (Table5) since larvae were more uniformly mixed throughout the plume layer. When K_z was high larvae acted more like passive particles transported by a depth-averaged current.



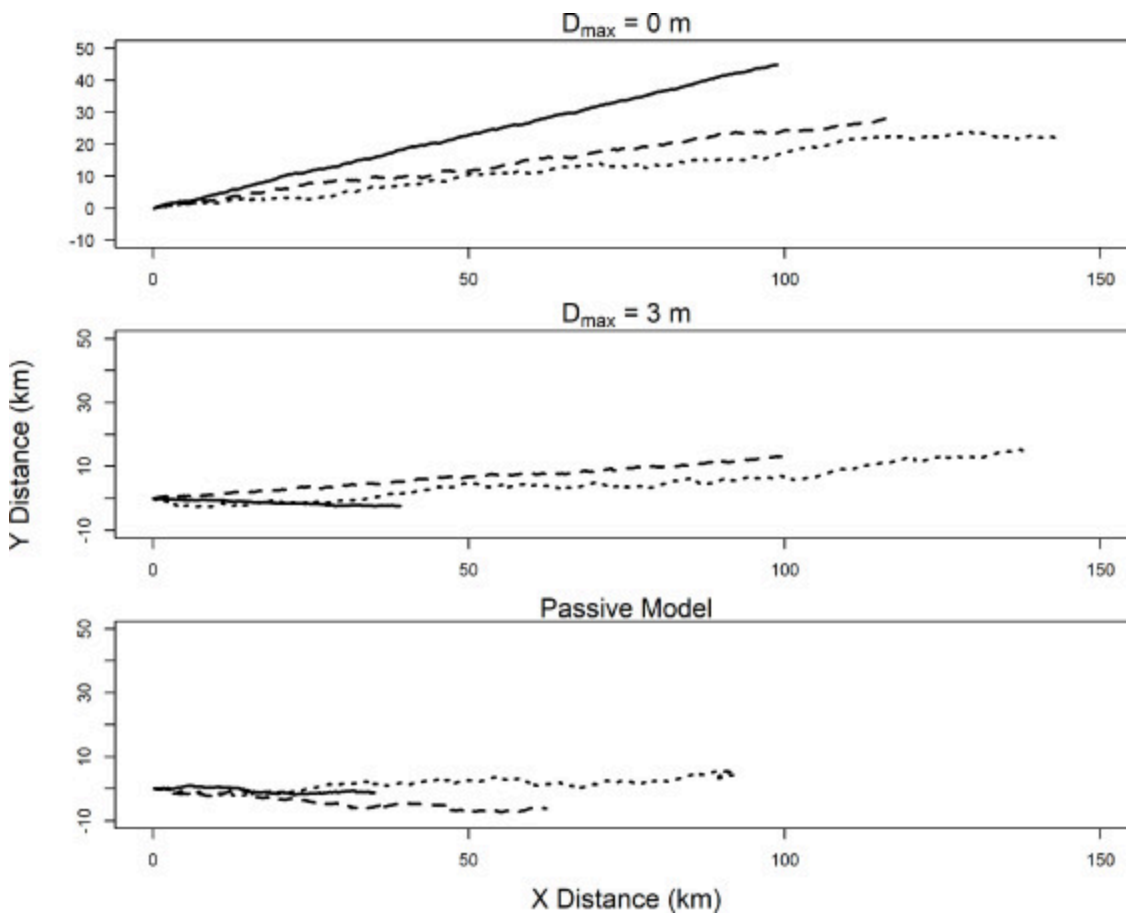
[Download: Download high-res image \(467KB\)](#)

[Download: Download full-size image](#)

Fig. 6. Frequency distribution of net transport distance on 10km bins for larval group O (black lines) and passive particles (grey lines). Panels show frequency distributions for scenarios with each combination of wind speed (rows) and D_{max} (columns).

Along-plume transport (X_{net}) was larger than cross-plume transport (Y_{net} ; Fig.4). Model configuration parameters had similar effects on X_{net} as they did to S . However, at an intermediate plume depth, particles experienced a reversal in cross-plume flow, resulting in a more southward trajectory than surface particles. The effect of this flow reversal was evident from a strong interaction between wind speed and D_{max} on Y_{net} (Fig.4). When $D_{max}=0m$, near-surface larvae had a smaller Y_{net} , and as wind speed and K_z increased, larvae experience near-zero depth-averaged V velocity. However, as D_{max} increased, stronger swimming larvae's behavior constrained them higher in the plume layer and were more

likely to be positioned near the flow reversal depth. Ultimately larvae with a deeper D_{max} experienced more southerly trajectories (Fig.7).



[Download: Download high-res image \(305KB\)](#)

[Download: Download full-size image](#)

Fig. 7. Example 2-dimensional horizontal trajectories of particles representative of median net transport from various model configurations with behavior (top and center) and as passive particles (bottom). Example trajectories for particles at 5 m s^{-1} (solid lines), 10 m s^{-1} (dashed lines), and 15 m s^{-1} (dotted lines) are also shown.

3.2. Passive particle scenarios

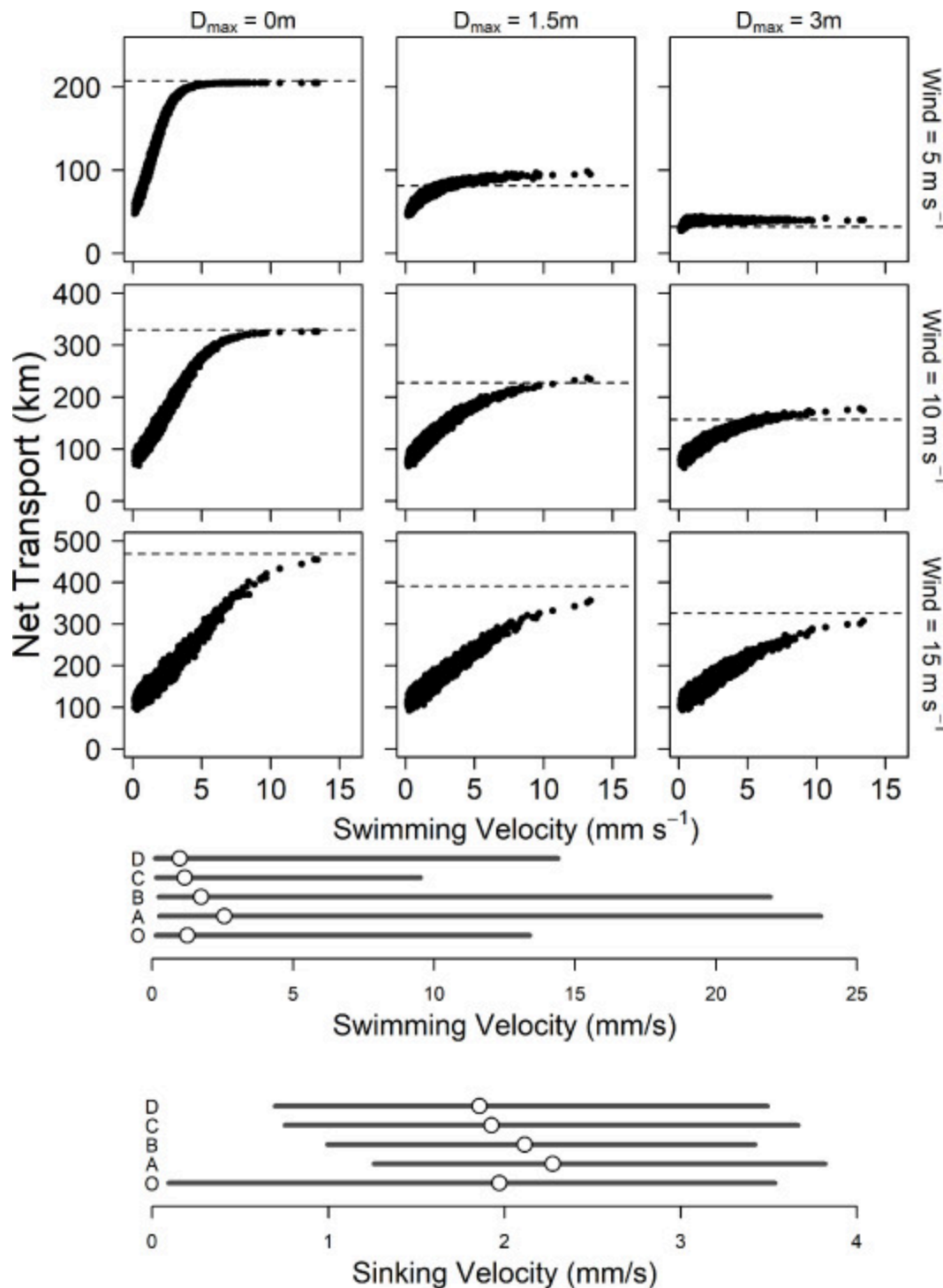
In passive particle scenarios, wind was a significant factor in determining net transport (ANOVA, $F=18,086$, $p \ll 0.001$), where faster winds increased net transport. This was expected since horizontal advection scaled with wind stress and vertical advection was stochastic. Passive particles became uniformly distributed with depth throughout the plume within 1 – 2h. There was a slight aggregation of particles at the pycnocline (Fig.5) caused by the rapid decrease in K_z to the background diffusivity. Over the course of the 4-day

simulation, particles had a deeper depth distribution in the lower layer but were still not uniformly distributed.

In all 45 configurations with behaving particles, the distribution of S and vertical position differed from analogous configurations with passive particles (K-S, $p \ll 0.001$), indicating that even simple surface-keeping behavior ($D_{max}=0\text{m}$) may significantly alter larval transport when turbulent mixing is present. Even when mixing was minimized (wind speed of 5m s^{-1}), behaving larvae with a D_{max} of 0m had a mean vertical position one tenth of passive particles. Additionally, the median S for all larval groups was greater than that of passive particles in the same physical conditions (Table 5). Behaving particles at a 5m s^{-1} wind speed and $D_{max}=3\text{m}$ behaved most like passive particles (Fig. 4). When D_{max} was closer to the plume depth, larvae spent more time in their sinking phase, had a deeper depth distribution, and had net transport (Fig. 6) and trajectories (Fig. 7) more like passive particles.

3.3. Swimming velocity and transport

Configurations with behaving particles showed that transport was related to larval swimming velocity and thus larval group. There was a positive non-linear relationship between S and W_{swim} whereby faster-swimming larvae were transported further, but this relationship asymptotes at a maximum transport distance (S_{max}) bounded by physical conditions and their D_{max} (Fig. 8). If $D_{max} > 0\text{m}$, this S_{max} is defined by the horizontal advection at one half of D_{max} due to the larvae's oscillating behavior. Larvae with higher W_{swim} travelled closer to S_{max} when wind speed was lower and $D_{max} > 0\text{m}$. The majority of larvae swam too slowly to reach S_{max} in most model configurations, as shown by their lower Pe , with the exception of configurations with the slowest wind speeds.

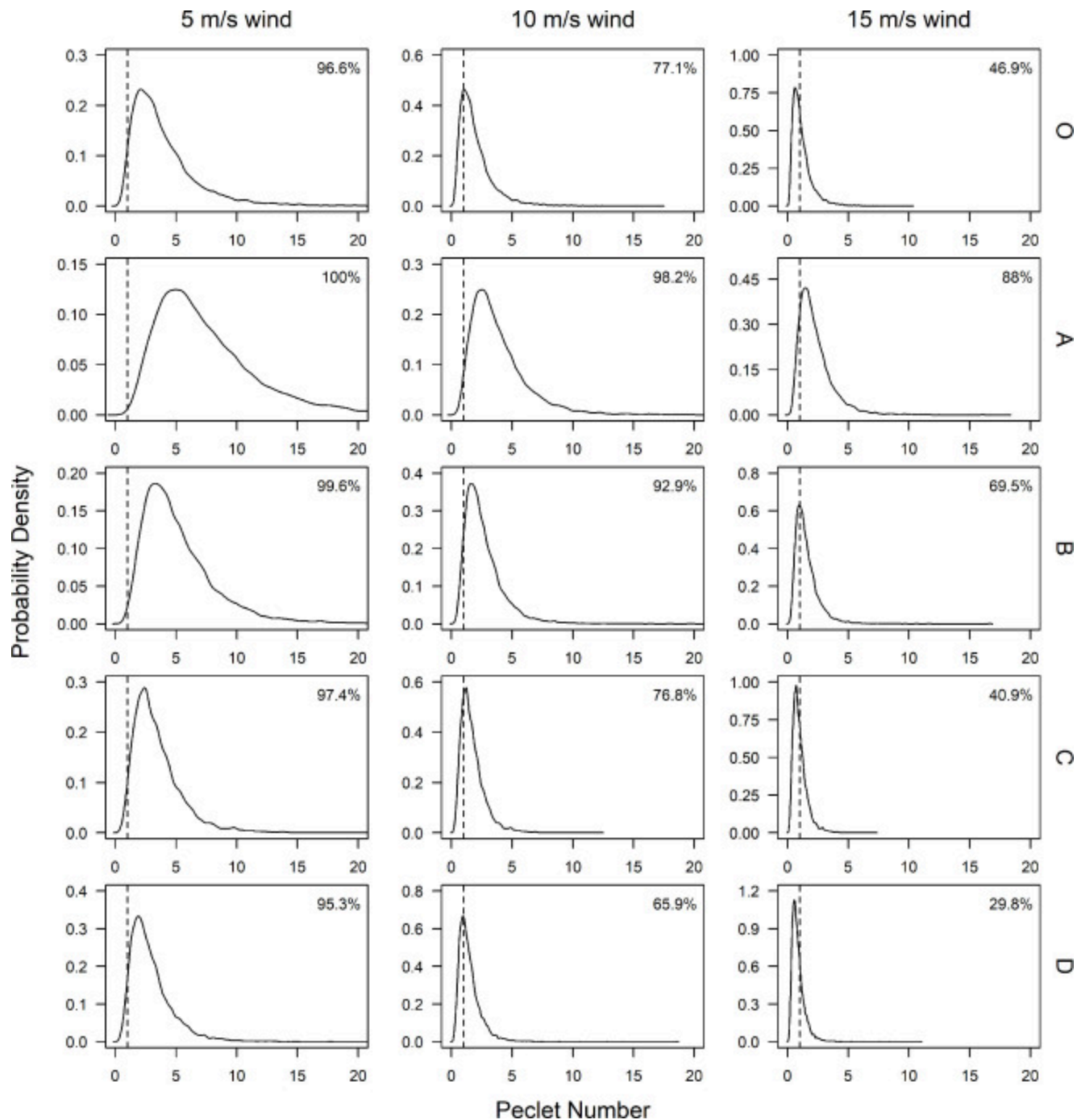


[Download: Download high-res image \(621KB\)](#)

[Download: Download full-size image](#)

Fig. 8. The net transport distance over 4 days for all particles in larval group O as a function of larval swimming velocity. Panels distinguish D_{max} (columns) and wind speed (rows). Dashed horizontal lines show the maximum transport possible for particles fixed at one half D_{max} for a given wind speed. Bottom panels show the range of swimming and sinking velocities for each larval group with open circles denoting the median.

The fraction of all simulated larvae whose Péclet number exceeded one was calculated (Fig.9). Pe depends on plume depth (constant in this model), larval swimming speeds, and vertical diffusivity and is not affected by the D_{max} parameter. Thus, Pe is a characteristic of larval group and wind scenario only. At a wind speed of 5 m s^{-1} , at least 95% of zoeae from all larval groups had a $Pe > 1$. Thus, zoeae had control over their vertical position when wind speeds are low. However, as wind speed increased the proportion of larvae with $Pe > 1$ decreased, and the difference in Pe proportion between broods is more apparent. When winds were 15 m s^{-1} , 88% of larvae the fastest swimming brood (A) and 30% of larvae from the slowest swimming brood (D) had $Pe > 1$. This disparity between broods explains why there is an increase in brood-level differences in transport at higher wind speeds. In no model configurations with behaving particles do all larvae have a $Pe < 1$, so broods never entirely act like passive particles. In fact, only at the fastest wind speed and for the slowest swimming broods (C and D) do a majority of the larvae have a $Pe < 1$.



[Download: Download high-res image \(814KB\)](#)

[Download: Download full-size image](#)

Fig. 9. Distributions of the Péclet number (Pe) for simulated larvae from each behavioral group (rows) and for each wind speed scenario (columns). Vertical dashed line show a Pe of 1, and the percentage of larvae with $Pe > 1$ is shown in the top right corner of each panel. Some distributions are truncated to allow ease of comparison.

4. Discussion

4.1. Larval behavior and transport

Though the idealized plume structure and Ekman dynamics in this model exclude other important physical processes, upwelling winds are the dominant process that drives surface waters in the nearshore mid-Atlantic Bight ([Lentz,2008](#); [Lentz and Largier,2006](#); [Rennie et al., 1999](#)). The simplicity of this model suited the scope of this study and facilitated the investigation of interactions between wind speed and larval behaviors. Even when hypothetical aspects of the larval behavior model are ignored (i.e. when $D_{max} > 0\text{m}$), larval traits still influenced transport via larvae's ability to counter vertical mixing. The presence of behaviors does not guarantee changes in transport, especially if larval swimming was not strong enough to counter turbulence. However, there was no model configuration where the majority of particles behaved as if they were passive particles, even at high wind speeds and strong turbulence. These results indicate that brood variation in *C. sapidus* zoeal swimming behavior observed by [Caracappa and Munroe\(2019\)](#) could result in brood-dependent larval transport.

Despite most zooplankton lacking the ability to control their horizontal position via swimming, many are able to exert control over their vertical position. Horizontal advection can vary substantially with depth (i.e. sheared flow), allowing vertical swimming behavior to alter larval trajectories in ways different than those predicted by passive transport alone ([Metaxas,2001](#); [Shanks,2009, 1995](#)). Behavior-driven differences in larval transport have been simulated in models of larval bivalves ([Munroe et al., 2018](#); [North et al., 2008](#)), corals ([Szmant and Meadows,2006](#)), and other decapod crustaceans ([Katz et al., 1994](#); [Moksnes et al., 2014](#)). The vertical distribution of zoeae should be more uniform when winds are stronger, but the response of *C. sapidus* zoeae may also be affected by turbulence. The results of this model align with field observations, where under relatively calm conditions, zoeae are heavily skewed towards the surface ([Provenzano,1983](#)). In contrast, to *C. sapidus*, other estuarine crab species' larvae develop within estuaries and exhibit selective tidal stream transport, undergoing diel vertical migrations over several meters ([Epifanio and Cohen,2016](#)). For *Carcinus maenas* ([Banas et al., 2009](#); [Moksnes et al., 2014](#)) more complex biophysical models show that this behavior results in a larger degree of control over horizontal position than in the case of this study, suggesting that while *C. sapidus* larvae behavior may influence transport, it is to a lesser degree than for other species. Since *C. sapidus* larvae maintain a position near the surface and field sampling may be difficult under stronger wind conditions, the potential influences of behavior may have been overlooked. Observations regarding the vertical distribution of zoeae as a function of wind speed or turbulence would fill critical data gaps and allow for further refinement of our behavioral model.

The nature of the D_{max} parameter and resulting vertical oscillations in the model are mostly hypothetical and presuppose a resting period that is triggered by depth. Though highly simplistic, centimeter-scale depth measurements at timescales of minutes are prohibitively difficult to measure in situ. In the case that larvae do not experience a prolonged passive sinking phase, D_{max} would be 0m. In still conditions, laboratory behavioral experiments have not been done with deep enough enclosures to identify a true D_{max} . Despite the underlying larval swimming behavior in all scenarios constrained to vertical oscillation, all model configurations showed that wind-driven mixing resulted in complex patterns in vertical position over time. The duration of either swimming or sinking phases varied greatly depending on the strength of the mixing and particles' swimming speed. Despite the uncertainty in parameterizing potential swimming behavior, brood-dependent transport distance was still seen for surface-keeping particles ($D_{max}=0m$).

Larval behaviors included in this model reflected observation, but they were based on experiments done under controlled and static conditions ([Caracappa and Munroe, 2019](#)). Realistically, *C. sapidus* larval behavior also varies with environmental conditions ([Forward and Cronin, 1980](#); [Sulkin et al., 1980](#)) and molt stage ([Sulkin et al., 1980](#)). However, behavioral responses to some potentially important environmental conditions (e.g. turbulence, salinity, temperature, light, food) have not been studied or lack information needed to generate distributions of individualized behaviors. These data gaps make it difficult to construct individual-based models using more complex physical conditions and refined behaviors. More experimental or in situ observations are needed to better understand the range of *C. sapidus* larval behaviors and how they can interact with dispersal processes.

4.2. Behavioral variation

The investigation of brood-dependent larval dispersal in zoeae stems from recent experimental work. Multivariate morphological differences between larval broods have been documented in both *C. sapidus* ([Caracappa and Munroe, 2018](#)) and *Pugettia quadridens* ([Tamura et al., 2017](#)), and brood-dependent mortality to stressors has been documented in *Lithodes santolla* ([DiSalvatore et al., 2020](#)). Brood effects in *C. sapidus* larvae have been shown to influence swimming behavior as well ([Caracappa and Munroe, 2019](#)). When incorporated into this model, the 2.5 fold difference in swimming velocity between broods, translated to a maximum 1.8 fold difference in transport distance. However, across all larvae, irrespective of brood, net transport distance varied by a factor of 2 during the slowest wind speeds. Larval swimming velocity possessed highly skewed distributions, which result in similarly skewed distributions of transport distance, such that faster-swimming larvae were transported

further than their slower-swimming analogues. The magnitude of swimming and behavioral effects are evident when compared against net transport for passive particles, which have shorter transport distances with narrower distributions. Brood effects were present in all configurations, but were smaller at decreased wind speed and deeper *D_{max}*. Thus brood effects (and behavioral effects in general) on transport may be situational and depend on local physical conditions.

The larval broods chosen for this study form a continuous, overlapping distribution of swimming velocity, but it is uncertain whether they are representative of the entire reproducing population. The presence of possible outlier broods (e.g. group A) suggests a small subset of the reproducing population could produce larvae more capable of maintaining a surface position, countering vertical mixing, and transporting further distances. It may be that outlier larvae end up dispersing to more distant settling habitats (founder individuals) by virtue of their swimming ability.

It is worth stressing that transport distance has limitations as a metric of successful dispersal. Successful recruitment of *C. sapidus* larvae is a relatively rare event, with estimates of over 99% mortality during larval development and dispersal ([McConaugha, 1992](#)). Past modeling efforts have identified that loss to advection (i.e. larval wastage) may be the largest component of mortality ([Garvine et al., 1997](#)). Larvae exported too far south along the MAB shelf may be advected outside suitable settlement habitat via the Gulf Stream. In fact, differences in transport potential between broods may simply indicate differences in dispersal strategy. Existing *C. sapidus* dispersal models suggest transport distances are highly variable, often with divergent dispersal patterns whereby some larvae are retained near their spawning location while others are transported much farther away ([Criales et al., 2019](#)). The larvae simulated here may reflect such recruitment strategies via the high variation in behavior. More complex models of shelf dynamics are needed to predict realistic dispersal trajectories and evaluate settling sites success across the population, and we recommend a consideration of behavioral variation in their construction. One difficulty in incorporating behaviors into individual-based larval dispersal models is in parameterizing individual responses to environmental conditions. Extensive observations and targeted experiments are needed, and even with decades of behavioral experiments, a comprehensive *C. sapidus* larval behavioral model has not been created. Our hypothetical model of *C. sapidus* larval transport and behavior allows for both individually-varying behaviors, and simulations suggest and maternal influences on behavior leading to behavior- and brood-dependent transport. Further experimental and modeling work is needed to identify whether such behavioral and maternal influence affect dispersal under more complex hydrographic conditions.

CRediT authorship contribution statement

Joseph C. Caracappa: Conceptualization, Methodology, Software, Formal analysis, Writing – original draft, Writing – review & editing, Visualization. **Daphne M. Munroe:** Methodology, Validation, Writing – review & editing, Supervision, Project administration, Funding acquisition. **Heidi L. Fuchs:** Methodology, Software, Writing – review & editing. **Robert J. Chant:** Methodology, Conceptualization, Writing – review & editing.

Declaration of Competing Interest

The authors declare the following financial interests/personal relationships which may be considered as potential competing interests:

Joseph Caracappa reports financial support was provided by Rutgers The State University of New Jersey.

Acknowledgements

We acknowledge P. Lopez-Duarte and P. Jivoff for their thoughtful feedback and revisions of this manuscript and M. Kozak for his technical assistance. J. Caracappa was supported by a graduate assistantship from the Department of Marine and Coastal Sciences at Rutgers University.

[Recommended articles](#)

Data availability

Data will be made available on request.

References

[Banas et al., 2009](#) N.S. Banas, P.S. McDonald, D.A. Armstrong
Green crab larval retention in Willapa Bay, Washington: an intensive
Lagrangian modeling approach
Estuaries Coasts, 32 (2009), pp. 893-905, [10.1007/s12237-009-9175-7](https://doi.org/10.1007/s12237-009-9175-7) ↗
[View in Scopus](#) ↗ [Google Scholar](#) ↗

[Caracappa and Munroe, 2019](#) J.C. Caracappa, D.M. Munroe

Variability in swimming behavior among broods of blue crab (*Callinectes sapidus*) zoeae

J. Exp. Mar. Bio. Ecol., 518 (2019), Article 151176, [10.1016/j.jembe.2019.151176](https://doi.org/10.1016/j.jembe.2019.151176) ↗



[View PDF](#) [View article](#) [View in Scopus](#) ↗ [Google Scholar](#) ↗

[Caracappa and Munroe, 2018](#) J.C. Caracappa, D.M. Munroe

Morphological variability among broods of first-stage blue crab (*Callinectes sapidus*) Zoeae

Biol. Bull., 235 (2018), pp. 123-133

[View article](#) [Crossref](#) ↗ [View in Scopus](#) ↗ [Google Scholar](#) ↗

[Costlow and Bookhout, 1959](#) J.D.J. Costlow, C.G. Bookhout

The larval development of *Callinectes Sapidus* Rathbun reared in the laboratory

Biol. Bull., 116 (1959), pp. 373-396

[Crossref](#) ↗ [Google Scholar](#) ↗

[Craig, 1996](#) P.D. Craig

Velocity profiles and surface roughness under breaking

J. Geophys. Res., 101 (1996), pp. 1265-1277

[View in Scopus](#) ↗ [Google Scholar](#) ↗

[Criales et al., 2019](#) M. Criales, L. Chérubin, R. Gandy, L. Garavelli, M. A Ghannami, C. Crowley

Blue crab larval dispersal highlights population connectivity and implications for fishery management

Mar. Ecol. Prog. Ser., 625 (2019), pp. 53-70, [10.3354/meps13049](https://doi.org/10.3354/meps13049) ↗

[View in Scopus](#) ↗ [Google Scholar](#) ↗

[Di Salvatore et al., 2020](#) P. Di Salvatore, H.J. Sacristán, M.P. Sotelano, F. Tapella, M. Gowland-Sainz, G.A. Lovrich

Southern King Crab larval survival: from intra and inter-female variations to a fishery-induced mortality

Can. J. Fish. Aquat. Sci., 11 (2020), pp. 1-11, [10.1139/cjfas-2020-0040](https://doi.org/10.1139/cjfas-2020-0040) ↗

[Google Scholar](#) ↗

[Epifanio, 1995](#) C.E. Epifanio

Transport of blue crab (*Callinectes sapidus*) larvae in the waters off Mid-Atlantic states

Bull. Mar. Sci., 57 (1995), pp. 713-725

[Google Scholar](#) ↗

[Epifanio and Cohen, 2016](#) C.E. Epifanio, J.H. Cohen

Behavioral adaptations in larvae of brachyuran crabs: a review

J. Exp. Mar. Bio. Ecol., 482 (2016), pp. 85-105, [10.1016/j.jembe.2016.05.006](#) ↗



[View PDF](#) [View article](#) [View in Scopus](#) ↗ [Google Scholar](#) ↗

[Epifanio and Garvine, 2001](#) C.E. Epifanio, R.W. Garvine

Larval transport on the Atlantic continental shelf of North America: a review

Estuar. Coast. Shelf Sci., 52 (2001), pp. 51-77, [10.1006/ecss.2000.0727](#) ↗



[View PDF](#) [View article](#) [View in Scopus](#) ↗ [Google Scholar](#) ↗

[Epifanio and Tilburg, 2008](#) C.E. Epifanio, C.E. Tilburg

Transport of blue crab larvae in the Middle Atlantic Bight: a wet and windy journey

J. Mar. Res., 66 (2008), pp. 723-749

[Crossref](#) ↗ [View in Scopus](#) ↗ [Google Scholar](#) ↗

[Fong and Geyer, 2001](#) D.A. Fong, R.W. Geyer

Response of a river plume during an upwelling favorable wind event

J. Geophys. Res. Ocean., 106 (2001), pp. 1067-1084, [10.1029/2000JC900134](#) ↗

[View in Scopus](#) ↗ [Google Scholar](#) ↗

[Forward and Cronin, 1980](#) R.B. Forward, T.W. Cronin

Tidal rhythms of activity and phototaxis of an Estuarine crab larvae

Biol. Bull., 158 (1980), pp. 295-303

[Crossref](#) ↗ [Google Scholar](#) ↗

[Forward and Buswell, 1989](#) R.J.B. Forward, C.U. Buswell

A comparative study of behavioral responses of larval decapod crustaceans to light and pressure

Mar. Behav. Physiol., 16 (1989), pp. 43-56

[Crossref](#) ↗ [Google Scholar](#) ↗

[Garvine et al., 1997](#) R.W. Garvine, C.E. Epifanio, C.C. Epifanio, K.-C. Wong

Transport and recruitment of blue crab larvae: a model with advection and mortality

Estuar. Coast. Shelf Sci., 45 (1997), pp. 99-111, [10.1006/ecss.1996.0161](#) ↗



[View PDF](#) [View article](#) [View in Scopus](#) ↗ [Google Scholar](#) ↗

[Giltz et al., 2020](#) S.M. Giltz, E.K. Grey, J. Gyory, D.S. Ko, R.W. Nero, C.M. Taylor

Estimating blue crab (*Callinectes sapidus*) larval release sites in the Gulf of Mexico using an oceanographic particle-tracking model

Bull. Mar. Sci., 96 (2020), pp. 563-576, [10.5343/bms.2018.0075](https://doi.org/10.5343/bms.2018.0075) ↗

[Google Scholar](#) ↗

[Jiang and Xia, 2016](#) L. Jiang, M. Xia

Dynamics of the Chesapeake Bay outflow plume: realistic plume simulation and its seasonal and interannual variability

J. Geophys. Res. Ocean., 121 (2016), pp. 1424-1445, [10.1002/2015JC011191](https://doi.org/10.1002/2015JC011191) ↗

[View in Scopus](#) ↗ [Google Scholar](#) ↗

[Johnson and Hess, 1990](#) D.F. Johnson, K.W. Hess

Numerical simulations of blue crab larval dispersal and recruitment

Bull. Mar. Sci., 46 (1990), pp. 195-213

[View in Scopus](#) ↗ [Google Scholar](#) ↗

[Johnson, 1985](#) D.R. Johnson

Wind-forced dispersion of blue crab larvae in the Middle Atlantic Bight

Cont. Shelf Res., 4 (1985), pp. 733-745, [10.1016/0278-4343\(85\)90039-1](https://doi.org/10.1016/0278-4343(85)90039-1) ↗

 [View PDF](#) [View article](#) [View in Scopus](#) ↗ [Google Scholar](#) ↗

[Johnson et al., 1984](#) Johnson, D.R., Hester, B.S., Mcconaugha, J.R., 1984. Studies of a wind mechanism influencing the recruitment of blue crabs in the Middle Atlantic Bight 3, 425–437.

[Google Scholar](#) ↗

[Karp-Boss et al., 1996](#) L. Karp-Boss, E. Boss, P.A. Jumars

Nutrient fluxes to planktonic osmotrophs in the presence of fluid motion

Oceanogr. Mar. Biol. An Annu. Rev., 34 (1996), pp. 71-107

[View in Scopus](#) ↗ [Google Scholar](#) ↗

[Katz et al., 1994](#) C.H. Katz, J.S. Cobb, M. Spaulding

Larval behavior, hydrodynamic transport, and potential offshore-to-inshore recruitment in the American lobster *Homarus americanus*

Mar. Ecol. Prog. Ser., 103 (1994), pp. 265-274, [10.3354/meps104265](https://doi.org/10.3354/meps104265) ↗

[View in Scopus](#) ↗ [Google Scholar](#) ↗

[Kingsford et al., 2002](#) M.J. Kingsford, J.M. Leis, A. Shanks, K.C. Lindeman, S.G. Morgan, J. Pineda

Sensory environments, larval abilities and local self-recruitment

Bull. Mar. Sci., 70 (2002), pp. 309-340, [10.1666/0022-3360\(2005\)079<0337:CFTNMO>2.0.CO;2](https://doi.org/10.1666/0022-3360(2005)079<0337:CFTNMO>2.0.CO;2) ↗

[View in Scopus ↗](#) [Google Scholar ↗](#)

[Large and Pond, 1980](#) W.G. Large, S. Pond

Open ocean momentum flux measurements in moderate to strong winds

J. Phys. Oceanogr., 11 (1980), pp. 324-336

[Google Scholar ↗](#)

[Lentz, 2008](#) S.J. Lentz

Observations and a model of the mean circulation over the Middle Atlantic Bight

J. Phys. Oceanogr., 38 (2008), pp. 1203-1221, [10.1175/2007JPO3768.1 ↗](#)

[View in Scopus ↗](#) [Google Scholar ↗](#)

[Lentz and Largier, 2006](#) S.J. Lentz, J. Largier

The influence of wind forcing on the Chesapeake Bay buoyant coastal current

J. Phys. Oceanogr., 36 (2006), pp. 1305-1316, [10.1175/JPO2909.1 ↗](#)

[View in Scopus ↗](#) [Google Scholar ↗](#)

[McConaugha, 1992](#) J. McConaugha

Decapod larvae: dispersal, mortality, and ecology. A working hypothesis

Am. Zool., 32 (1992), pp. 512-523

[Crossref ↗](#) [Google Scholar ↗](#)

[McEdward, 1995](#) McEdward, L., 1995. Ecology of marine invertebrate larvae. CRC Press.

[Google Scholar ↗](#)

[Metaxas, 2001](#) A. Metaxas

Behaviour in flow: perspectives on the distribution and dispersion of meroplanktonic larvae in the water column

Can. J. Fish. Aquat. Sci., 58 (2001), pp. 86-98, [10.1139/f00-159 ↗](#)

[View in Scopus ↗](#) [Google Scholar ↗](#)

[Metaxas and Saunders, 2009](#) A. Metaxas, M. Saunders

Quantifying the “Bio-” components in biophysical models of larval transport in marine benthic invertebrates: advances and pitfalls

Biol. Bull., 216 (2009), pp. 257-272, [10.2307/25548159 ↗](#)

[View in Scopus ↗](#) [Google Scholar ↗](#)

[Moksnes et al., 2014](#) P.-O. Moksnes, H. Corell, K. Tryman, R. Hordoir, P.R. Jonsson

Larval behavior and dispersal mechanisms in shore crab larvae (*Carcinus maenas*): local adaptations to different tidal environments?

Limnol. Oceanogr., 59 (2014), pp. 588-602, [10.4319/lo.2014.59.2.0588](https://doi.org/10.4319/lo.2014.59.2.0588) ↗

[View in Scopus ↗](#) [Google Scholar ↗](#)

[Munroe et al., 2018](#) D.M. Munroe, D. Haidvogel, J.C. Caracappa, J.M. Klinck, E.N. Powell, E.E. Hofmann, B.V. Shank, D.R. Hart

Modeling larval dispersal and connectivity for Atlantic sea scallop (*Placopecten magellanicus*) in the Middle Atlantic Bight

Fish. Res., 208 (2018), pp. 7-15, [10.1016/j.fishres.2018.06.020](https://doi.org/10.1016/j.fishres.2018.06.020) ↗

 [View PDF](#) [View article](#) [View in Scopus ↗](#) [Google Scholar ↗](#)

[North et al., 2008](#) E.W. North, Z. Schlag, R.R. Hood, M. Li, L. Zhong, T. Gross, V.S. Kennedy
Vertical swimming behavior influences the dispersal of simulated oyster larvae in a coupled particle-tracking and hydrodynamic model of Chesapeake Bay

Mar. Ecol. Prog. Ser., 359 (2008), pp. 99-115, [10.3354/meps07317](https://doi.org/10.3354/meps07317) ↗

[View in Scopus ↗](#) [Google Scholar ↗](#)

[Pineda et al., 2007](#) J. Pineda, J.A. Hare, S. Sponaugle
Larval transport and dispersal in the coastal ocean and consequences for population connectivity

Oceanography, 20 (2007), pp. 22-39, [10.5670/oceanog.2007.27](https://doi.org/10.5670/oceanog.2007.27) ↗

[View in Scopus ↗](#) [Google Scholar ↗](#)

[Pineda and Reynolds, 2018](#) J. Pineda, N. Reynolds
Larval Transport in the Coastal Zone: Biological and Physical Processes (2018), pp. 141-159, [10.1093/oso/9780198786962.003.0011](https://doi.org/10.1093/oso/9780198786962.003.0011) ↗

[Google Scholar ↗](#)

[Pollard et al., 1973](#) R.T. Pollard, P.B. Rhines, O.R.Y. Thompson
The deepening of the wind-mixed layer

Geophys. Fluid Dyn., 4 (1973), pp. 381-404

[Crossref ↗](#) [Google Scholar ↗](#)

[Pond and Pickard, 1983](#) S. Pond, G.L. Pickard
Introductory Dynamical Oceanography

Pergamon Press (1983)

[Google Scholar ↗](#)

[Price et al., 1978](#) J.F. Price, C.N.K. Mooers, J.C. Van Leer

Observation and simulation of storm-induced mixed-layer deepening

J. Phys. Oceanogr., 8 (1978), pp. 582-599

[View in Scopus ↗](#) [Google Scholar ↗](#)

[Provenzano, 1983](#) A. Provenzano

Vertical distribution of first stage larvae of the blue crab, *Callinectes sapidus*, at the mouth of Chesapeake Bay

Estuar. Coast. Shelf Sci., 16 (1983), pp. 489-499



[View PDF](#) [View article](#) [View in Scopus ↗](#) [Google Scholar ↗](#)

[R Core Team, 2015](#) R. Core Team, 2015. R: a language and environment for statistical computing.

[Google Scholar ↗](#)

[Rennie et al., 1999](#) S.E. Rennie, J.L. Largier, S.J. Lentz

Observations of a pulsed buoyancy current downstream of Chesapeake Bay

J. Geophys. Res. Ocean., 104 (1999), pp. 18227-18240, [10.1029/1999jc900153 ↗](#)

[View in Scopus ↗](#) [Google Scholar ↗](#)

[Richman et al., 1987](#) J.G. Richman, R.A. de Szoeke, R.E. Davis

Measurements of near-surface shear in the Ocean

J. Geophys. Res., 92 (1987), pp. 2851-2858

[View in Scopus ↗](#) [Google Scholar ↗](#)

[Ross and Sharples, 2004](#) O.N. Ross, J. Sharples

Recipe for 1-D Lagrangian particle tracking models in space-varying diffusivity

Limnol. Oceanogr. Methods, 2 (2004), pp. 289-302

[Crossref ↗](#) [View in Scopus ↗](#) [Google Scholar ↗](#)

[Ruzecki, 1981](#) Ruzecki, E.P., 1981. Temporal and spatial variations of the Chesapeake Bay plume.

[Google Scholar ↗](#)

[Shanks, 2009](#) A.L. Shanks

Pelagic larval duration and dispersal distance revisited

Biol. Bull., 216 (2009), pp. 373-385, [10.2307/25548167 ↗](#)

[View in Scopus ↗](#) [Google Scholar ↗](#)

[Shanks, 1995](#) A.L. Shanks

Mechanisms of cross-shelf dispersal of larval invertebrates

L.R. McEdward (Ed.), *Ecology of Marine Invertebrate Larvae* (Ed.), CRC Press, New York (1995), pp. 323-368

[Google Scholar](#) ↗

[Shanks and Brink, 2005](#) A.L. Shanks, L. Brink

Upwelling, downwelling, and cross-shelf transport of bivalve larvae: test of a hypothesis

Mar. Ecol. Prog. Ser., 302 (2005), pp. 1-12, [10.3354/meps302001](#) ↗

[View in Scopus](#) ↗ [Google Scholar](#) ↗

[Simons et al., 2013](#) R.D. Simons, D.A. Siegel, K.S. Brown

Model sensitivity and robustness in the estimation of larval transport: a study of particle tracking parameters

J. Mar. Syst., 119–120 (2013), pp. 19-29, [10.1016/j.jmarsys.2013.03.004](#) ↗



[View PDF](#) [View article](#) [View in Scopus](#) ↗ [Google Scholar](#) ↗

[Smyth, 1980](#) P.O. Smyth

Callinectes (decapoda: portunidae) larvae in the middle atlantic bight, 1975-77

Fish. Bull., 78 (1980), pp. 251-265

[Google Scholar](#) ↗

[Sponaugle et al., 2002](#) S. Sponaugle, R.K. Cowen, A. Shanks, S.G. Morgan, J.M. Leis, J. Pineda, G.W. Boehlert, M.J. Kingsford, K.C. Lindeman, C. Grimes, J.L. Munro

Predicting self-recruitment in marine populations: biophysical correlates and mechanisms

Bull. Mar. Sci., 70 (2002), pp. 341-375

[View in Scopus](#) ↗ [Google Scholar](#) ↗

[Sulkin, 1984](#) S.D. Sulkin

Behavioral basis of depth regulation in the larvae of brachyuran crabs

Mar. Ecol. Prog. Ser., 15 (1984), pp. 181-205, [10.3354/meps015181](#) ↗

[Google Scholar](#) ↗

[Sulkin et al., 1980](#) S.D. Sulkin, W. van Heukelem, P. Kelly, L. van Heukelem

The behavioral basis of larval recruitment in the crab *Callinectes sapidus* Rathbun: a laboratory investigation of ontogenetic changes in geotaxis and

barokinesis

Biol. Bull., 159 (1980), pp. 402-417

[Crossref ↗](#) [Google Scholar ↗](#)

[Szmant and Meadows, 2006](#) A.M. Szmant, M.G. Meadows

Developmental changes in coral larval buoyancy and vertical swimming behavior: implications for dispersal and connectivity

Proc. 10th Int. Coral Reef Symp (2006), pp. 431-437

[Google Scholar ↗](#)

[Tamura et al., 2017](#) H. Tamura, J.M. Landeira, S. Goshima

Morphological and morphometric variability in the zoea I larvae of *Pugettia quadridens* (De Haan, 1839): looking for reliable characters for taxonomic studies on the genus *Pugettia* Dana, 1851 (Majoidea: epialtidae)

Zootaxa, 4226 (2017), pp. 264-272

[View in Scopus ↗](#) [Google Scholar ↗](#)

[Tilburg et al., 2009a](#) C.E. Tilburg, A.I. Dittel, C.E. Epifanio

High concentrations of blue crab (*Callinectes sapidus*) larvae along the offshore edge of a coastal current: effects of convergent circulation

Fish. Oceanogr., 18 (2009), pp. 135-146, [10.1111/j.1365-2419.2009.00502.x ↗](#)

[View in Scopus ↗](#) [Google Scholar ↗](#)

[Tilburg et al., 2009b](#) C.E. Tilburg, A.I. Dittel, C.E. Epifanio

High concentrations of blue crab (*Callinectes sapidus*) larvae along the offshore edge of a coastal current: effects of convergent circulation

Fish. Oceanogr., 18 (2009), pp. 135-146, [10.1111/j.1365-2419.2009.00502.x ↗](#)

[View in Scopus ↗](#) [Google Scholar ↗](#)

[Tilburg et al., 2007](#) C.E. Tilburg, A.I. Dittel, C.E. Epifanio

Retention of crab larvae in a coastal null zone

Estuar. Coast. Shelf Sci., 72 (2007), pp. 570-578, [10.1016/j.ecss.2006.11.030 ↗](#)

 [View PDF](#) [View article](#) [View in Scopus ↗](#) [Google Scholar ↗](#)

[Tilburg et al., 2005](#) C.E. Tilburg, J.T. Reager, M.M. Whitney

The physics of blue crab larval recruitment in Delaware Bay: a model study

J. Mar. Res., 63 (2005), pp. 471-495, [10.1357/0022240053693699 ↗](#)

[View in Scopus ↗](#) [Google Scholar ↗](#)

[Visser, 1997](#) A.W. Visser

Using random walk models to simulate the vertical distribution of particles in a turbulent water column

Mar. Ecol. Prog. Ser., 158 (1997), pp. 275-281

[Crossref ↗](#) [View in Scopus ↗](#) [Google Scholar ↗](#)

[Welch et al., 1999](#) J.M. Welch, R.J.B. Forward, P.A. Howd

Behavioral responses of blue crab *Callinectes sapidus* postlarvae to turbulence: implications for selective tidal stream transport

Mar. Ecol. Prog. Ser, 179 (1999), pp. 135-143

[Crossref ↗](#) [View in Scopus ↗](#) [Google Scholar ↗](#)

[White, 1974](#) F.M. White

Viscous Fluid Flow

McGraw-Hill, New Yor (1974)

[Google Scholar ↗](#)

[Whitney and Garvine, 2005](#) M.M. Whitney, R.W. Garvine

Wind influence on a coastal buoyant outflow

J. Geophys. Res., 110 (2005), pp. 1-15, [10.1029/2003JC002261 ↗](#)

[View in Scopus ↗](#) [Google Scholar ↗](#)

[Yankovsky et al., 2000](#) A.E. Yankovsky, R.W. Garvine, A. Münchow

Mesoscale currents on the inner new jersey shelf driven by the interaction of buoyancy and wind forcing

J. Phys. Oceanogr., 30 (2000), pp. 2214-2230,

[10.1175/1520-0485\(2000\)030<2214:MCOTIN>2.0.CO;2 ↗](#)

[View in Scopus ↗](#) [Google Scholar ↗](#)

Cited by (0)

© 2023 The Authors. Published by Elsevier B.V.



All content on this site: Copyright © 2024 Elsevier B.V., its licensors, and contributors. All rights are reserved, including those for text and data mining, AI training, and similar technologies. For all open access content, the Creative Commons licensing terms apply.

